Research Article Vol. 30, No. 5 / 28 Feb 2022 / Optics Express 6556
Optics EXPRESS

Study on the single-mode condition for x-cut LNOI rib waveguides based on leakage losses

XIA RONG YU,[1] MENG KE WANG,[1] JUN HUI LI,[1] JIE YUN WU,[1] ZHE FENG HU,[1,2] AND KAI XIN CHEN[1,*]

[1] School of Optoelectronic Science and Engineering, University of Electronic Science and Technology of China, Chengdu 611731, China
[2] Wuhan National Laboratory for Optoelectronics, Huazhong University of Science and Technology, Wuhan, 430074, China
[*] chenkx@uestc.edu.cn

Abstract: Lithium niobate-on-insulator (LNOI) has recently emerged as a promising material platform for high-density and advanced photonics integrated circuits (PICs). And single-mode waveguides (SMW) are the most basic building blocks for structuring various PICs. In this paper, single-mode conditions (SMCs) for shallowly etched LNOI rib waveguides in x-cut LNOI wafer are investigated with the finite element method (FEM) in consideration of the lateral leakage and the magic width for the first time, to our best knowledge. Our results indicate that due to the lateral leakage and the magic width these shallowly etched x-cut LNOI rib waveguides have unique and complex SMCs. Our method and results provide a guidance in designing low-loss LNOI SMW and high-performance PICs.

1. Introduction

Lithium niobate (LN) crystal, an outstanding material platform for achieving high-performance electro-optic (EO), acousto-optic (AO), and nonlinear optic devices, is embracing a significant revolution from traditional wafer to novel thin film on insulator wafer [1,2]. Sub-micrometer-thickness crystalline LN thin films bonded on insulator (usually silica), i.e., lithium niobate on insulator (LNOI), not only inherits the excellent characteristics of LN crystal, but also enable compact high-index-contrast waveguides, making it a promising platform for the development of advanced, high-density EO photonic integrated circuits (PICs) [1–4].

Waveguides, especially the single-mode waveguides (SMWs), are the backbone of various LNOI PICs. Nowadays, hybrid waveguides and monolithic waveguides are two main types of the LNOI waveguides [2,4]. Hybrid waveguides are based on rib-loading or heterogeneous bonding and implemented by etching the easier etched material [5–8], which exempt the necessity of LN etching. However, only a portion of optical field in hybrid waveguides is confined in the LN film, resulting in weaker nonlinear and EO effects. In addition, the devices using hybrid waveguides are quite sensitive to the change of temperature due to different thermal expansion coefficients between the LN and the loaded material [2]. Thus, the hybrid waveguides are not optimal option for the LNOI PICs. Monolithic waveguide, however, is implemented by etching the LN film into rib structure, which can achieve strong confinement and low loss for the light wave traveling inside and, hence, is considered an optimal option for the LNOI PICs [2,9]. Up to now, various LNOI PICs realized with rib waveguides, such as, EO modulator [10–13], EO tunable interleaver [14], ring resonators [15–17], optical amplifier [18], tunable Bragg grating filter [19], second-harmonic generator [20], and entangled photon pair generator [21] have been demonstrated. However, a systematic and in-depth investigation of single-mode conditions (SMCs) for the LNOI rib waveguides has not been carried out. Recently, Y. Li et al. reported their investigation for the SMCs of the LNOI rib waveguides based on the leakage from the core modes to the same polarized slab modes [22]. However, the leakage to the orthogonally polarized

#451842 https://doi.org/10.1364/OE.451842
Journal © 2022 Received 20 Dec 2021; revised 28 Jan 2022; accepted 4 Feb 2022; published 14 Feb 2022

Optics EXPRESS

slab modes, which has also important impacts on the SMCs, does not involved in their work. In comparison, the SMCs for SOI rib waveguides, another important building block based on silicon (Si) material platform for PICs, have been widely and deeply investigated [23–25]. Unlike SOI rib waveguides formed with isotropic Si crystal, the LNOI rib waveguides formed with anisotropic LN crystal exhibit larger material and waveguide birefringence, which, in conjunction with the unique lateral leakage that rib waveguides possess [26], leads to quite complicated SMCs. Considering that SMW is essential building block in PICs, it is quite necessary to further investigate SMCs for the LNOI rib waveguides.

In this paper, we deeply investigate the SMCs for the shallowly etched x-cut, y-propagation LNOI rib waveguides, a type of waveguides most widely used in the LNOI PICs, using a commercial mode solver (COMSOL) based on the finite element method (FEM). For simplicity, the LNOI rib waveguides in the following refer to this shallow etch type except where otherwise stated. Compared with the work in [22], our investigation for the SMCs of the LNOI rib waveguides involves the above two types of leakage. To our best knowledge, it is the first time to take lateral leakage losses of the higher order modes into consideration when investigating SMCs of the LNOI rib waveguides. The impacts of the morphological parameters of the LNOI rib waveguides and the operation wavelengths on the SMCs are also investigated and presented.

2. Waveguide structure

The cross-sectional view of our investigated LNOI rib waveguide is shown schematically in Fig. 1, which consists of one ridge and two side slabs on both sides of the ridge. Such waveguide structure supports two types of guided modes. One is the modes confined in the ridge (ridge modes), labeled conventionally as E^x_{ij} or E^z_{ij} ($i, j = 1, 2, 3 \ldots$), where subscript indicates the mode order and superscript the direction of the maximum electric field component, the other is the modes confined in the slab (slab modes), labeled conventionally as TE_m or TM_m ($m = 0, 1, 2, \ldots$), where TE indicates transverse electric field and TM transverse magnetic field. According to the coordinate system shown in Fig. 1, the E^z_{ij} and TE_m modes have the same polarization along z direction (TE polarization), while the E^x_{ij} and TM_m modes have the same polarization along x direction (TM polarization). When the ridge mode E^x_{ij} or E^z_{ij} leaks into the slab, it will be converted into slab modes TM_m or TE_m. The morphological parameters of the investigated LNOI rib waveguide are also shown in Fig. 1, in which h is the waveguide height (i.e., the thickness of the initial LN thin film), w the top width of the ridge, h_e the etch depth, h_s the side-slab height, h_c the thickness of the cladding layer, θ the side wall angle. Usually, the SiO_2 buffer layer is thick enough (3-5 μm) to avoid any field penetration into the underlying substrate. The refractive indices of the materials in the core, buffer, and cladding layers are denoted as n_1, n_2, and n_3, respectively, as shown in Fig. 1, and at the most commonly used 1550 nm wavelength, $n_1 = 2.1376$ for the TE polarization and 2.2111 for the TM polarization, and $n_2 = n_3 = 1.444$ for both polarizations. It should be pointed out that the waveguide structure shown in Fig. 1 facilitates placement of the tuning electrodes on the two sides of the ridge to utilize efficiently the

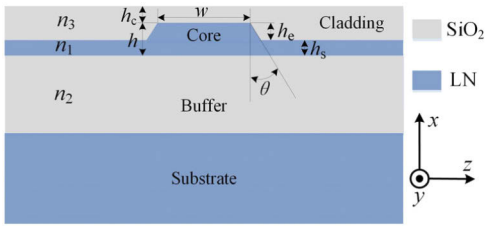

Fig. 1. Cross-sectional view of the LNOI rib waveguide investigated in this paper.

Optics EXPRESS

maximum EO coefficient γ_{33}. And on this basis, the maximum EO interaction can be achieved by optimizing the morphological parameters of the waveguide [2]. Thus, such waveguide structure is widely used in the LNOI PICs.

3. Method

To achieve single-mode propagation in the LNOI rib waveguides, two mechanisms can be employed. The first one is by adopting deep etching to achieve the cut-off of the first order modes E^x_{21} and E^z_{21}, just like the single-mode mechanism used in rectangular waveguide. The second one is by adopting shallow etching to make the ridge to accommodate the fundamental modes E^x_{11} and E^z_{11} and the first modes E^x_{21} and E^z_{21}, but the waveguide parameters will be controlled precisely to achieve the leakage of the E^x_{21} and E^z_{21} modes into the two side slabs, and ultimately, only the fundamental modes of the ridge in the waveguide. It needs to be pointed out that due to the anisotropy of LN two types of leakage, including the leakage to the same polarized modes and to the orthogonally polarized modes, could happen in the LNOI rib waveguides. Obviously, compared with the first mechanism, the second one is capable of realizing not only a lower coupling loss between the waveguide and the standard SMF due to a larger waveguide cross section, but also a lower propagation loss induced by the side-wall roughness due to a smaller side-wall area, and therefore most widely adopted in the design of the LNOI PICs. In view of this, our investigation for the SMCs focuses on these shallowly etched LNOI rib waveguides. Note that the word "shallow" and "deep" in this paper are just used to differentiate between the above two mechanisms, does not mean that the etch depth is really shallow.

The maximum etching depth h_{emax} that can still realize single-mode propagation in the shallowly etched LNOI rib waveguides are investigated with the FEM (COMSOL). Here, two cases need to be considered, one is the unetched slab (corresponding to thickness h) is thick enough to accommodate the first order modes TE_1 and TM_1, the other is the unetched slab only accommodates the fundamental modes TE_0 and TM_0. For the former, single-mode propagation requires that the TE_1 and TM_1 modes of the unetched slab can leak into the etched slab (corresponding to thickness h_s). For the latter, single-mode propagation requires that the ridge modes E^z_{21} and E^x_{21} can leak into the etched slab. In view of the fact that the effective indices of the E^z_{21} and E^x_{21} modes are related to the ridge width w, to get h_{emax} for this case, a quite narrow width of $w = 400$ nm is used here. At last, in consideration that the above leakage of the high-order mode is due to the fact that its effective index is equal to that of the same polarized fundamental mode of the etched slab, then h_{emax} can be obtained.

Figure 2 presents the calculated h_{emax} with the FEM for different h from 400 to 1000 nm under the condition that $h_c = 200$ nm, the operation wavelength is 1550 nm, and the air cladding is also taken into account. For typical thickness $h = 400$, 600, and 900 nm, the calculated h_{emax} are 357, 503, and 626 nm for the TE polarization, respectively, and 299, 520, and 546 nm for the TM polarization, respectively. According to the above analysis, for the LNOI rib waveguides with $h_e < h_{emax}$, single-mode propagation is possible, but whether that happens depends on the leakage losses of the E^x_{21} and E^z_{21} modes determined by the w, h and the polarization state of the light wave, which will be discussed in the section 4.

The above analysis only involves the leakage to the same polarized modes. However, shallowly etched rib waveguides have a unique characteristic of the lateral leakage due to the coupling of the two orthogonally polarized modes at the ridge boundary [26]. Because of the high index contrast, the ridge mode has a strong longitudinal electric field component along the waveguide axis, while the orthogonal slab mode can propagate at any angle relative to the waveguide axis. If the effective index of the ridge mode is smaller than that of the orthogonal slab mode, quite strongly phase-matched coupling between the ridge mode and the orthogonal slab mode may happen, depending on the propagation angle of the orthogonal slab mode. For the SOI rib waveguides, only the TM-like guided mode (here the label of the mode follows that used in references) can be

Optics EXPRESS

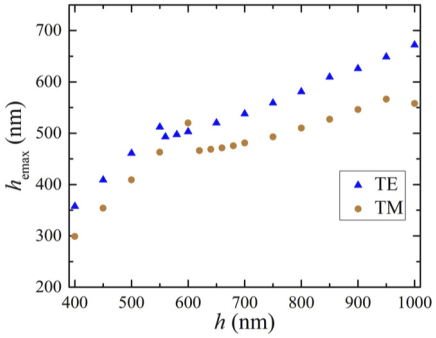

Fig. 2. Calculated h_{emax} for LNOI rib waveguides corresponding to the TE and TM polarizations at different h.

coupled to the TE slab mode, resulting in lateral leakage, which has been investigated deeply in [27,28]. However, for the LNOI rib waveguides, due to its strong materials and waveguide birefringence the E^x_{21} or E^z_{21} mode could be coupled, respectively, to the orthogonal TE_0 or TM_0 mode, and hence, become leaky [29].

Obviously, the lateral leakage will result in large losses of the ridge modes. However, at special widths, resonant cancellation of lateral leakage can be realized and hence dramatically reduce the lateral leakage losses of the ridge modes, these special widths are called magic widths [26]. The lateral leakage losses of the fundamental ridge modes have been investigated in design of LNOI waveguide [29] and polarizer [30]. Practically, similar principle can also be utilized to design single-mode LNOI rib waveguide by engineering the lateral leakage losses of the E^x_{21} and E^z_{21} modes. If the morphological parameters of the LNOI rib waveguide make the lateral leakage happen and the leakage loss is larger than a certain level, such as 1 dB/mm used in this paper, then single-mode propagation in rib waveguide can be considered to have been achieved. Such a loss level is need to determine whether the losses of the higher order modes are large enough to make them disappear completely after propagating a certain length inside the waveguide. The loss level can be adjusted in accordance with the specific applications.

The complex propagation constant β of the ridge mode in the LNOI rib waveguides can be calculated with FEM by applying perfectly matched layer (PML) boundaries, and then the lateral leakage loss can be obtained by [29]

$$Leakage\ loss = 8.686\mathrm{Im}\{\beta\}\ [\mathrm{dB/m}] \tag{1}$$

4. Results and Discussion

In this section, the SMCs for the LNOI rib waveguides are investigated by combining modal dispersion curves with the lateral leakage losses of the E^z_{21} and E^x_{21} modes. As aforementioned, the lateral leakages of the ridge modes E^z_{21} and E^x_{21} are related to the effective indices of the fundamental TE_0 and TM_0 slab modes, respectively. In view of this, the dispersion curves of the TE_0 and TM_0 modes of the LNOI slab waveguides were calculated with FEM at 1550 nm wavelength for different h_s and fixed $h_c = 0$, 200, and 400 nm, respectively. The calculated results are shown in Fig. 3. It can be seen that for different h_c, the two polarizations have almost the same effective index around $h_s = 660$ nm, and for the h_s less (larger) than this value the effective index of the TM_0 is less (larger) than that of the TE_0. Thus, for the LNOI rib waveguides formed with $h > 660$ nm, both lateral leakage from the E^z_{21} mode to the TM_0 mode and from the E^x_{21} mode to the TE_0 mode are possible, but which happens depends on the etch depth h_e. However, for the LNOI rib waveguides formed with $h < 660$ nm, only lateral leakage from the E^x_{21} mode to the TE_0 happens. In addition, from Fig. 3, for the cases of $h_s > 660$ nm, three curves of the

Optics EXPRESS

TM_0 mode corresponding to $h_c = 0$, 200, and 400 nm are very close to one another, and for the cases of $h_s < 660$ nm, three curves of the TE_0 mode also show similar feature, indicating that the cladding thickness h_c only has a slight impact on the SMCs.

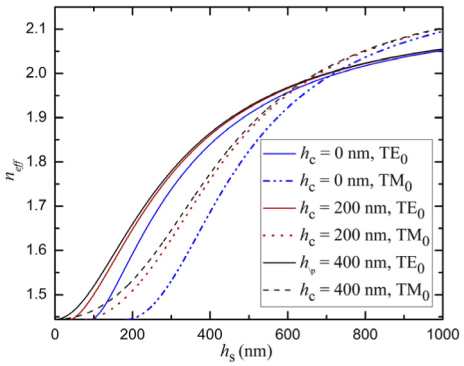

Fig. 3. Effective indices of the TE_0 and TM_0 modes of the LNOI slab waveguides as a function of the slab thickness h_s at different $h_c = 0$, 200, 400 nm, respectively.

In consideration of the impact of the slab thickness h_s on the lateral leakage, we select three typical LN film thicknesses of $h = 400$, 600, and 900 nm as examples to investigate the SMCs of the LNOI rib waveguides under the condition of $h_c = 200$ nm, $\theta = 22°$, and $\lambda = 1550$ nm. Obviously, for the LNOI rib waveguides with $h_e < h_{emax}$, the achievement of single-mode propagation depends mainly on the ridge width w. Thus, for the sake of clarity, we define $w(h_e)$ as the critical width to describe the SMCs of the LNOI rib waveguides having etch depth h_e. Here $w(h_e)$ corresponds to the ridge width with which both the E^x_{21} and E^z_{21} modes are leaky and the corresponding leakage loss is larger than 1 dB/mm.

For the case of $h = 900$ nm, h_{emax} are 626 and 546 nm for the TE and TM polarizations, respectively. Here two cases of $h_e = 540$ and 90 nm are presented to illustrate how to get $w(h_e)$. For the case of $h_e = 540$ nm, the dispersion curves of the ridge and slab modes involved are calculated at different w from 0.42 μm to 3.0 μm and shown in Fig. 4(a). Meanwhile, the leakage losses of the E^z_{21} and E^x_{21} modes are also calculated at different w from 0.42 μm to 1.0 μm and shown in Fig. 4(b). It needs to be pointed out that although the LNOI rib waveguide in this case accommodate the E^z_{12} and E^x_{12} modes, both have leakage losses much larger than 1 dB/mm (not shown in Fig. 4(b)) and, hence, are not taken into consideration here. From Fig. 4(a), the E^z_{21} mode is cut-off at $w < w_z = 0.74$ μm, i.e., leaks to the same polarized TE_0 mode, as indicated by the mode field distribution of the E^z_{21} mode shown in the inset of Fig. 4(a), while the E^x_{21} mode is cut-off at $w < w_x = 0.42$ μm, i.e., leaks to the same polarized TM_0 mode. Therefore, if only the leakage to the same polarized modes are taken into consideration, the SMC require $w < w_x$ (= 0.42 μm). However, when the leakage to the orthogonally polarized modes, i.e, the leakage from the E^x_{21} mode to the TE_0 mode, are taken into consideration, the SMC will be determined by the cut-off width of the E^x_{21} mode, and the SMW width will be enlarged to w_z (= 0.74 μm), as shown in Fig. 4(a). Further, at $w = w_z = 0.74$ μm, the effective index of the E^x_{21} mode is smaller than that of the TE_0 mode as shown in Fig. 4(a), meeting the cut off condition, but the E^x_{21} mode has a quite low loss of 3.27×10^{-4} dB/mm at this width because w_z is very close to the magic width w_m (= 0.763 μm) of the E^x_{21} mode, as shown in the inset of Fig. 4(b). Thus, to achieve the cut-off of the E^x_{21} mode based on a larger loss of more than 1 dB/mm, the width w should be smaller than w_{x1} (= 0.66 μm). At last, based on the above facts, $w(h_e = 540\text{ nm}) = 0.66$ μm can be obtained.

Next, for the case of $h_e = 90$ nm, the calculated dispersion curves and leakage losses of the modes involved are shown in Figs. 4(c) and 4(d), respectively. Over the range from 0.5 μm to 3.0 μm, the E^z_{21} mode is cut-off and the E^z_{11} mode leaks to the TM_0 slab mode as shown in

Optics EXPRESS

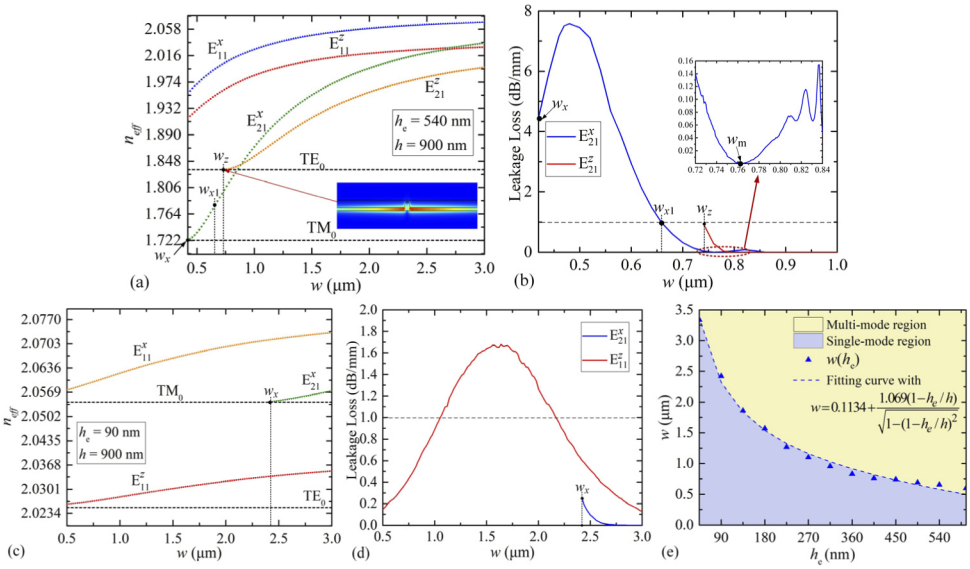

Fig. 4. Calculated (a) and (c) modal dispersion curves, (b) and (d) modal leakage losses at different w, (a) and (b) $h_e = 540$ nm, (c) and (d) $h_e = 90$ nm, as well as (e) $w(h_e)$ and the fitting curve of $w(h_e)$ at different h_e, of the LNOI rib waveguides formed with 900-nm thick LN film at $\theta = 22°$, $h_c = 200$ nm, and $\lambda = 1550$ nm.

Fig. 4(c). Meanwhile, the E^x_{21} mode is cut-off when $w < w_x$ =2.42 μm and its leakage loss is far less than the given level of 1 dB/mm when $w > w_x$, as show in Fig. 4(d). In view of these facts, $w(h_e = 90\text{ nm}) = 2.42$ μm can be obtained. Note that although the E^z_{11} mode is leaky as shown in Fig. 4(c), it has different leakage losses from 0.15 to 1.68 dB/mm over the width range from 0.5 to 2.42 μm due to the magic width, and at some special width, such as around 0.5 μm as shown in Fig. 4(d), the propagation of the E^z_{11} mode with a quite low loss is possible. Thus, the LNOI SMW at these widths can support both the E^z_{11} and E^x_{11} modes propagation with low loss.

With the same method, $w(h_e)$ for other etch depth h_e can be obtained, and the fitting curve formed by all of these $w(h_e)$ that separates multi-mode region and single-mode region, as shown in Fig. 4(e), can be obtained. Obviously, below each $w(h_e)$, there are a group of SMWs that have the same h_e but different and smaller w.

Next, for the case of $h = 400$ nm, $h_e = 40$ nm is selected as an example and the calculated dispersion curves and leakage losses of the modes involved are shown in Figs. 5(a) and 5(b), respectively. It can be seen that if only the leakage to the same polarized modes are taken into consideration, the SMC require $w < w_x$ (= 1.72 μm). However, in consideration that over the range from 0.5 μm to 3 μm, the E^x_{21} modes leaks to the orthogonal TE_0 slab mode, the SMW width can be enlarged to w_z (= 2.52 μm), corresponding to the cut-off width of the E^z_{21} mode, as shown in Fig. 5(a). At the same time, the leakage losses of the E^x_{21} mode are greater than 1 dB/mm when $w < w_{x1}$ (= 2.8 μm) as shown in Fig. 5(b). Thus, $w(h_e = 40\text{ nm}) = 2.52$ μm can be obtained. It needs to be pointed out here that over the whole single-mode region from 0.5 μm to 2.52 μm, the E^x_{11} mode leaks to the TE_0 mode with different leakage losses at different width w and has a maximum loss at $w = 0.9$ μm and a minimum loss at $w = 2.3$ μm, i.e., the magic width of the E^x_{11} mode. Based on these facts, the LNOI SMW supporting both the E^z_{11} and E^x_{11} modes or only supporting the E^z_{11} mode can be obtained by choosing suitable ridge width w.

Further, by applying the above method, we calculated $w(h_e)$ and investigated the SMCs for other etch depth h_e for this case of $h = 400$ nm. The results are shown in Fig. 5(c), which exbibits

Optics EXPRESS

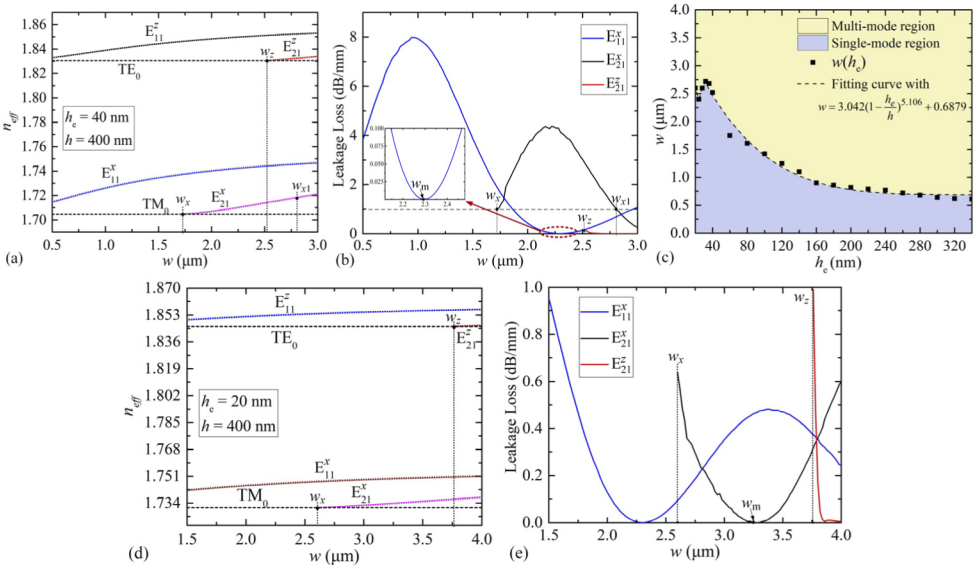

Fig. 5. Calculated (a) and (d) modal dispersion curves, (b) and (e) modal leakage losses at different w, (a) and (b) $h_e = 40$ nm, (d) and (e) $h_e = 20$ nm, as well as (c) $w(h_e)$ and the fitting curve of $w(h_e)$ at different h_e, of the LNOI rib waveguides formed with 400-nm thick LN film at $\theta = 22°$, $h_c = 200$ nm, and $\lambda = 1550$ nm.

unique SMC characteristics, that is the $w(h_e)$ decrease firstly and then increase in the range of $h_e = 20$ to 36 nm. The reason that causes this phenomenon can be accounted by an example of $h_e = 20$ nm. Figures 5(d) and 5(e) show respectively the calculated dispersion curves and leakage losses of the modes involved at $h_e = 20$ nm. It can be seen that the E^x_{21} mode leaks to the TE_0 slab mode in the range of w =2.61 to 4.0 μm, as shown in Fig. 5(d). but the leakage losses are between ~0 dB/mm (at magic width $w_m = 3.25$ μm) and 0.66 dB/mm (at $w_x = 2.61$ μm). In view of the fact that these losses are less than the given level of 1 dB/mm, the LNOI rib waveguide is multi-mode in this region in accordance with the previous stipulation. Meanwhile, from Fig. 5(d), E^x_{21} mode will be cut-off when $w < 2.61$ μm, therefore, $w(h_e = 20$ nm) should be somewhat smaller than 2.61 μm for this situation. Thus we set $w(h_e = 20$ nm) = 2.6 μm here.

For the case of $h = 600$ nm, the calculated dispersion curves and leakage losses of the modes involved at $h_e = 240$ nm are shown in Figs. 6(a) and 6(b), respectively. As shown in Fig. 6(a), the leakage to the same polarized modes require $w < w_x$ (= 0.72 μm), while the leakage from the E^x_{21} mode to the orthogonally polarized TE_0 mode leads to $w < w_z$ (= 0.94 μm). If the given loss level of 1 dB/mm is taken into account, then from the leakage losses of the E^z_{21} and E^x_{21} modes shown in Fig. 6(b), $w(h_e = 240$ nm) = w_{z1} = 1.09 μm can be obtained. However, because the magic width of the E^x_{21} mode is at $w_m = 0.77$ μm and the leakage losses of the E^x_{21} mode are smaller than 1 dB/mm from w_x (= 0.72 μm) to w_{x1} (= 0.86 μm), as shown in Fig. 6(b) and its inset, the range from $w = 0.72$ μm to 0.86 μm need to be excluded from single-mode region. With the same method, we can get $w(h_e)$ and the fitting curve of $w(h_e)$ at different h_e from 30 to 450 nm, above the fitting curve of $w(h_e)$ is multi-mode region, while below it is single-mode region except a belt of multi-mode region, as shown in Fig. 6(c).

The above three examples indicate that because of the lateral leakage loss and the magic width the LNOI rib waveguides have unique and complex SMCs, determined by the LN thin film thickness h, the etch depth h_e, and the ridge width w. It is difficult to describe SMCs of the LNOI rib waveguides by using an inequality, as used for SOI waveguides in [23–25]. Thus, to obtain

Optics EXPRESS

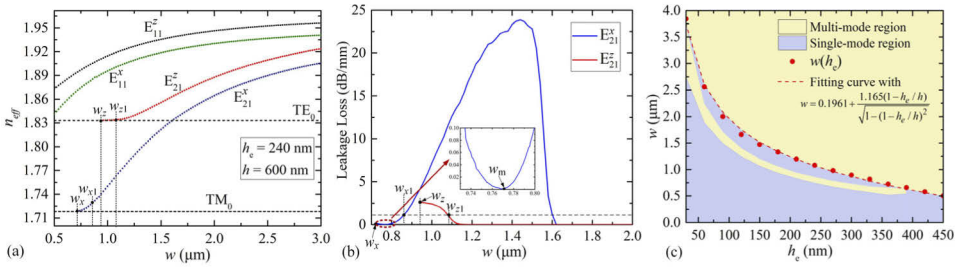

Fig. 6. Calculated (a) modal dispersion curves, (b) modal leakage losses at different w, and (c) $w(h_e)$ and the fitting curve of $w(h_e)$ at different h_e of the LNOI rib waveguides formed with 600-nm thick LN film at $\theta = 22°$, $h_c = 200$ nm, and $\lambda = 1550$ nm.

the SMC of the LNOI rib waveguide with given parameters, one need to investigate the modal dispersion curves and lateral leakage losses of the waveguide specifically.

At last, for the case of $h = 600$ nm, the impact of parameters h_c, θ, and λ on the $w(h_e)$ of the LNOI rib waveguides are also investigated with the above method over the etch depth range from 30 to 450 nm. The calculated values of $w(h_e)$ for the cases of $h_c = 0$ (no SiO_2 cover layer), 200, and 400 nm at fixed $\theta = 22°$ and λ=1550 nm are shown in Fig. 7(a), which indicates that with the increase of h_e, the impact of the thickness h_c of the SiO_2 cover layer on the $w(h_e)$ becomes gradually noteworthy. This is because the increases in the h_e and h_c lead to the decline in the confinement of the waveguide for the light wave. Meanwhile, the calculated $w(h_e)$ for the cases of $\theta = 18°$, 20° and 22° at $h_c = 200$ nm and λ=1550 nm indicates that these three cases of θ have almost the same impact on the SMCs, as shown in Fig. 7(b). Similarly, the calculated $w(h_e)$ for the cases of λ=1530, 1550, 1610 nm at fixed $h_c = 200$ nm and $\theta = 22°$ indicate that the above operation wavelengths only have a slight impact on the SMCs of the waveguide, as shown in Fig. 7(c).

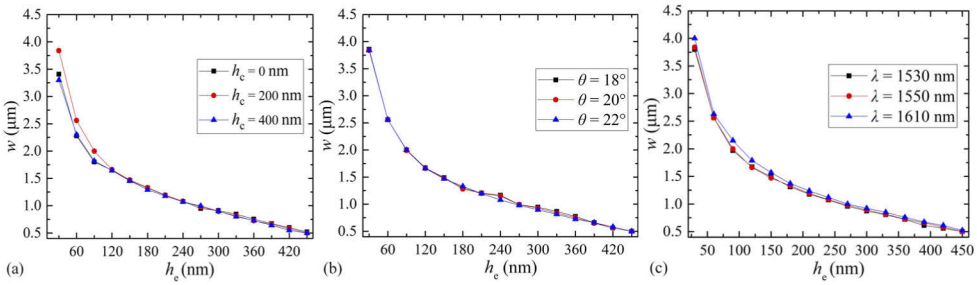

Fig. 7. Calculated $w(h_e)$ for the LNOI rib waveguides formed with 600-nm thick LN film for different cases, (a) $h_c = 0$, 200, 400 nm, respectively, and $\theta = 22°$, $\lambda = 1550$ nm, (b) $\theta = 18°$, 20°, 22°, respectively, and $h_c = 200$ nm, $\lambda = 1550$ nm, (c) $\lambda = 1530$, 1550, 1610 nm, respectively, and $\theta = 22°$, $h_c = 200$ nm.

5. Conclusion

We have investigated and obtained the SMCs of the LNOI rib waveguides formed with three typical-thickness LN film by combining the modal dispersion curves with the lateral leakage losses of the first order modes. Our results indicate that the single-mode propagation in shallowly etched LNOI rib waveguides can be realized by controlling the waveguide parameters precisely so as to achieve the leakage of the first order ridge modes into the two side slabs. And the

Optics EXPRESS

SMCs of these LNOI rib waveguides are mainly determined by the thickness of the LN thin film, the etch depth, and the width of the ridge, while the thickness of the cladding layer, the side wall angle, and the operation wavelength within a certain range only have slight impact on the SMCs. Moreover, it is quite difficult to describe the SMCs of these LNOI rib waveguides with a mathematical equation because they exhibit quite complex modal dispersions and leakage characteristics determined by the strong birefringence of LN and the specific structural parameters of the waveguide. One has to get the SMCs of each LNOI rib waveguide by investigating its modal dispersions and leakage losses. We believe that the above method and results can provide a guidance in designing low-loss LNOI SMW and high-performance PICs.

Funding. National Natural Science Foundation of China (62075027, U20A20165); Key Research and Development Program of Sichuan Province (2020YFSY0003); Wuhan National Laboratory for Optoelectronics (2019WNLOKF001); Fundamental Research Funds for the Central Universities (ZYGX2019J050, ZYGX2020ZB015).

Disclosures. The authors declare that there are no conflicts of interest related to this article.

Data availability. Data underlying the results presented in this paper are not publicly available at this time but may be obtained from the authors upon reasonable request.

References

1. G. Poberaj, H. Hu, W. Sohler, and P. Günter, "Lithium niobate on insulator (LNOI) for micro-photonic devices," Laser Photonics Rev. **6**(4), 488–503 (2012).
2. D. Zhu, L. Shao, M. Yu, R. Cheng, B. Desiatov, C. J. Xin, Y. Hu, J. Holzgrafe, S. Ghosh, A. Shams-Ansari, E. Puma, N. Sinclair, C. Reimer, M. Zhang, and M. Lončar, "Integrated photonics on thin-film lithium niobate," Adv. Opt. Photon. **13**(2), 242–352 (2021).
3. Y. Qi and Y. Li, "Integrated lithium niobate photonics," Nanophotonics **9**(6), 1287–1320 (2020).
4. A. Boes, B. Corcoran, L. Chang, J. Bowers, and A. Mitchell, "Status and Potential of Lithium Niobate on Insulator (LNOI) for Photonic Integrated Circuits," Laser Photonics Rev. **12**(4), 1700256 (2018).
5. A. Rao, A. Patil, J. Chiles, M. Malinowski, S. Novak, K. Richardson, P. Rabiei, and S. Fathpour, "Heterogeneous microring and Mach-Zehnder modulators based on lithium niobate and chalcogenide glasses on silicon," Opt. Express **23**(17), 22746–22752 (2015).
6. L. Chang, Y. Li, N. Volet, L. Wang, J. Peters, and J. E. Bowers, "Thin film wavelength converters for photonic integrated circuits," Optica **3**(5), 531–535 (2016).
7. P. O. Weigel, J. Zhao, K. Fang, H. Al-Rubaye, D. Trotter, D. Hood, J. Mudrick, C. Dallo, A. T. Pomerene, A. L. Starbuck, C. T. DeRose, A. L. Lentine, G. Rebeiz, and S. Mookherjea, "Bonded thin film lithium niobate modulator on a silicon photonics platform exceeding 100 GHz 3-dB electrical modulation bandwidth," Opt. Express **26**(18), 23728–23739 (2018).
8. A. N. R. Ahmed, S. Nelan, S. Shi, P. Yao, A. Mercante, and D. W. Prather, "Subvolt electro-optical modulator on thin-film lithium niobate and silicon nitride hybrid platform," Opt. Lett. **45**(5), 1112–1115 (2020).
9. K. Luke, P. Kharel, C. Reimer, L. He, M. Loncar, and M. Zhang, "Wafer-scale low-loss lithium niobate photonic integrated circuits," Opt. Express **28**(17), 24452–24458 (2020).
10. C. Wang, M. Zhang, X. Chen, M. Bertrand, A. Shams-Ansari, S. Chandrasekhar, P. Winzer, and M. Loncar, "Integrated lithium niobate electro-optic modulators operating at CMOS-compatible voltages," Nature **562**(7725), 101–104 (2018).
11. M. He, M. Xu, Y. Ren, J. Jian, Z. Ruan, Y. Xu, S. Gao, S. Sun, X. Wen, L. Zhou, L. Liu, C. Guo, H. Chen, S. Yu, L. Liu, and X. Cai, "High-performance hybrid silicon and lithium niobate Mach-Zehnder modulators for 100 Gbit s^{-1} and beyond," Nat. Photonics **13**(5), 359–364 (2019).
12. P. Kharel, C. Reimer, K. Luke, L. He, and M. Zhang, "Breaking voltage–bandwidth limits in integrated lithium niobate modulators using micro-structured electrodes," Optica **8**(3), 357–363 (2021).
13. M. Jin, J. Chen, Y. Sua, P. Kumar, and Y. Huang, "Efficient electro-optical modulation on thin-film lithium niobite," Opt. Lett. **46**(8), 1884–1887 (2021).
14. X. P. Li, K. X. Chen, and L. F. Wang, "Compact and electro-optic tunable interleaver in lithium niobate thin film," Opt. Lett. **43**(15), 3610–3613 (2018).
15. A. Guarino, G. Poberaj, D. Rezzonico, R. Degl'Innocenti, and P. Günter, "Electro-optically tunable microring resonators in lithium niobate," Nat. Photonics **1**(7), 407–410 (2007).
16. M. Zhang, C. Wang, R. Cheng, A. Shams-Ansari, and M. Lončar, "Monolithic ultra-high-Q lithium niobate microring resonator," Optica **4**(12), 1536–1537 (2017).
17. X. Liu, P. Ying, X. Zhong, J. Xu, Y. Han, S. Yu, and X. Cai, "Highly efficient thermo-optic tunable micro-ring resonator based on an LNOI platform," Opt. Lett. **45**(22), 6318–6321 (2020).
18. Z. Chen, Q. Xu, K. Zhang, W. Wong, D. Zhang, E. Y. Pun, and C. Wang, "Efficient erbium-doped thin-film lithium niobate waveguide amplifiers," Opt. Lett. **46**(5), 1161–1164 (2021).

Optics EXPRESS

19. K. Abdelsalam, E. Ordouie, M. G. Vazimali, F. A. Juneghani, P. Kumar, G. S. Kanter, and S. Fathpour, "Tunable dual-channel ultra-narrowband Bragg grating filter on thin-film lithium niobite," Opt. Lett. **46**(11), 2730–2733 (2021).
20. J. Zhao, M. Rüsing, U. A. Javid, J. Ling, M. Li, Q. Lin, and S. Mookherjea, "Shallow-etched thin-film lithium niobate waveguides for highly-efficient second-harmonic generation," Opt. Express **28**(13), 19669–19682 (2020).
21. J. Zhao, C. Ma, M. Rüsing, and S. Mookherjea, "High quality entangled photon pair generation in periodically poled thin-film lithium niobate waveguides," Phys. Rev. Lett. **124**(16), 163603 (2020).
22. Y. Li, T. Lan, D. Yang, and Z Wang, "Re-analysis of single-mode conditions for thin-film lithium niobate rib waveguides," Results in Phys. **30**, 104824 (2021).
23. J. Lousteau, D. Furniss, A. B. Seddon, T. M. Benson, A. Vukovic, and P. Sewell, "The single-mode condition for silicon-on-insulator optical rib waveguides with large cross section," J. Lightwave Technol. **22**(8), 1923–1929 (2004).
24. B. A. Dorin and W. N. Ye, "Conditions for single-mode and birefringence free ultrasmall SOI rib waveguides at 1310 nm," J. Lightwave Technol. **31**(21), 3420–3424 (2013).
25. H. Huang, K. Liu, B. Qi, and V. J. Sorger, "Re-Analysis of single mode conditions for silicon rib waveguides at 1550 nm wavelength," J. Lightwave Technol. **34**(16), 3811–3817 (2016).
26. T. G. Nguyen, A. Boes, and A. Mitchell, "Lateral Leakage in Silicon Photonics: Theory, Applications, and Future Directions," IEEE J. Sel. Topics Quantum Electron. **26**(2), 1–13 (2020).
27. M. A. Webster, R. M. Pafchek, A. Mitchell, and T. L. Koch, "Width Dependence of Inherent TM-Mode Lateral Leakage Loss in Silicon-On-Insulator Ridge Waveguides," IEEE Photonics Technol. Lett. **19**(6), 429–431 (2007).
28. T. G. Nguyen, R. S. Tummidi, T. L. Koch, and A. Mitchell, "Rigorous Modeling of Lateral Leakage Loss in SOI Thin-Ridge Waveguides and Couplers," IEEE Photonics Technol. Lett. **21**(7), 486–488 (2009).
29. E. Saitoh, Y. Kawaguchi, K. Saitoh, and M. Koshiba, "A design method of lithium niobate on insulator ridge waveguides without leakage loss," Opt. Express **19**(17), 15833–15842 (2011).
30. E. Saitoh, Y. Kawaguchi, K. Saitoh, and M. and Koshiba, "TE/TM-Pass Polarizer Based on Lithium Niobate on Insulator Ridge Waveguide," IEEE Photonics J. **5**(2), 6600610 (2013).